

On the computation of momentum distributions within wavepacket propagation calculations

Bernold Feuerstein and Uwe Thumm

Department of Physics, Kansas State University, Manhattan, KS 66506, USA

Received 28 October 2002

Published 4 February 2003

Online at stacks.iop.org/JPhysB/36/707

Abstract

We present a new method to extract momentum distributions from time-dependent wavepacket calculations. In contrast to established Fourier transformation of the spatial wavepacket at a fixed time, the proposed ‘virtual detector’ method examines the time dependence of the wavepacket at a fixed position. In first applications to the ionization of model atoms and the dissociation of H_2^+ , we find a significant reduction of computing time and are able to extract reliable fragment momentum distributions by using a comparatively small spatial numerical grid for the time-dependent wavefunction.

1. Introduction

Numerical wavefunction propagation for solving the time-dependent Schrödinger equation has been used extensively in order to describe the dynamics of strongly perturbed systems (Hermann and Fleck 1988, Kosloff 1994, Borisov *et al* 1999, Thumm 2002). Especially in the area of laser–matter interactions at high intensities, this method is currently applied to photoionization and photodissociation of few-particle systems such as the helium atom or small molecules, where the low or reduced dimensionality of the problem makes time-dependent calculations of this type feasible (Kulander *et al* 1996, Walsh *et al* 1998, Liu *et al* 2000, Lein *et al* 2000, Parker *et al* 2001, Bandrauk and Chelkowski 2001). Usually, the propagation is carried out in coordinate space and yields integral information about the considered process, e.g. total dissociation or ionization rates. However, if one desires to compare the calculation to differential experimental data such as momentum or kinetic energy distributions of the fragments, one has to extract these distributions from the outgoing wavepackets. A well established method is Fourier transformation (FT) which projects the wavefunction onto momentum eigenfunctions at a fixed time. The finite width of the momentum distributions gives rise to a significant dispersion of the wavepackets in coordinate space. Thus, a large numerical grid and long propagation times are required to get the full momentum information and to make the Fourier integrals converge. This becomes a serious computing time problem for systems of higher dimensionality. If the asymptotic behaviour of the continuum wavefunction

is analytically known, this problem can be avoided. Using analytical propagation for the asymptotic part of the wavefunction, the size of the numerical grid can be kept rather small (Keller 1995).

In this paper, we propose a new method to extract momentum distributions without propagation of the wavepacket over a large numerical grid. Here, the time dependence of the wavepacket at a *fixed* position is the source of the momentum information. Due to the analogy of this procedure to an experimental situation, we call this the ‘virtual detector’ (VD) method. The paper is structured as follows. After the general formulation, we demonstrate this method analytically as well as numerically for Gaussian wavepackets in one dimension. Next, we give numerical examples for the one-dimensional (1D) dissociation of H_2^+ following a Franck–Condon transition from the H_2 ground state and for the strong-field ionization of a 1D model hydrogen atom. We use atomic units throughout this paper, unless indicated otherwise.

2. General formulation of the ‘virtual detector’ method

The principles of quantum mechanics tell us that the wavefunction in any representation contains complete information about the considered system. As an example, the momentum distribution of a wavepacket Ψ is given by

$$|\Phi(\mathbf{k})|^2 = \left| (2\pi)^{-3/2} \int \Psi(\mathbf{r}) \exp(-i\mathbf{k}\mathbf{r}) \, d\mathbf{r} \right|^2, \quad (1)$$

i.e. by FT of the wavepacket’s coordinate space representation $\Psi(\mathbf{r})$. Thus, the momentum information is based on the global behaviour of Ψ in coordinate space. In many applications, transition rates which are related to the motion of wavepackets in coordinate space like ionization and dissociation (Kulander *et al* 1996, Chelkowski *et al* 1996, Dundas *et al* 1999) or reactive scattering (Neuhauser 1992) have been derived from the outgoing flux of the wavepacket through a given surface. The time-integrated flux corresponds to the probability of the corresponding ionization, dissociation or reaction channel. Using absorbing walls, comparatively small numerical grids can be used and, thus, the computing time can be significantly reduced. Here, we wish to extract information about the momentum distribution from the *time dependence* of an outgoing wavepacket at a *fixed position* in coordinate space. The input for FT is the *spatial dependence* of the wavefunction at a *fixed time*, i.e. the end of the propagation.

For the following considerations, we rewrite the wavefunction in the form

$$\Psi(\mathbf{r}, t) = A(\mathbf{r}, t) \exp(i\phi(\mathbf{r}, t)) \quad (2)$$

with a real, time-dependent amplitude $A(\mathbf{r}, t)$ and a real, time-dependent phase $\phi(\mathbf{r}, t)$. At a given position \mathbf{r}_d , $\phi(\mathbf{r}, t)$ contains information about the momentum distribution. To reveal this information, we consider the current density \mathbf{j} at \mathbf{r}_d of outgoing particles with mass μ ,

$$\mathbf{j}(\mathbf{r}_d, t) = \frac{\rho(\mathbf{r}_d, t)}{\mu} \nabla\phi(\mathbf{r}_d, t) \quad \text{with } \rho(\mathbf{r}_d, t) = |A(\mathbf{r}_d, t)|^2. \quad (3)$$

The (probability) current density can be interpreted as the product of the probability density ρ and a ‘local’ velocity \mathbf{v} at position \mathbf{r}_d which corresponds to the momentum

$$\mathbf{k}(\mathbf{r}_d, t) = \mu\mathbf{v} = \nabla\phi(\mathbf{r}_d, t). \quad (4)$$

The simplest example is an outgoing monochromatic plane wave $\Psi(\mathbf{r}, t) = (2\pi)^{-3/2} \exp[i(\mathbf{k}\mathbf{r} - \omega t)]$ where the phase gradient is directly related to the momentum \mathbf{k} . Similar to an experimental time-of-flight set-up, we now have to apply a ‘binning’ or ‘histogramming’ procedure in order to derive the momentum distribution dN/dk . In order

to keep this formulation transparent, we consider here the 1D case. Having the VD located at x_d , for each time t , we get the momentum $k(x_d, t)$. After time integration, the probability for finding the number of ‘events’ ΔN with momenta k within a small interval Δk around a momentum value k_j is given by

$$\Delta N(k_j) = \Delta k \int_0^\infty dt j(x_d, t) \begin{cases} 1 & \text{for } k \in [k_j - \frac{\Delta k}{2}, k_j + \frac{\Delta k}{2}] \\ 0 & \text{else.} \end{cases} \quad (5)$$

In the limit of an infinitesimal interval length dk , the ‘box’ distribution in (5) becomes a δ distribution,

$$\left. \frac{dN}{dk} \right|_{k'} = \int_0^\infty dt j(x_d, t) \delta(k' - k(x_d, t)). \quad (6)$$

The implicit time dependence of the argument of the δ distribution can be transformed into an explicit time dependence according to

$$\left. \frac{dN}{dk} \right|_{k'} = \sum_m \int_0^\infty dt j(x_d, t) \frac{\delta(t - t_m)}{|\frac{dk}{dt}(t_m)|} \quad t_m : k(t_m) = k' \quad (7)$$

$$= \frac{j(x_d, t(k'))}{|\frac{dk}{dt}(t(k'))|}. \quad (8)$$

Equation (7) can be reduced to (8) if $j(x_d, t)$ has dominant contributions only for sufficiently large t . This applies in the example below (section 3.1), where $k(t)$ is a monotonous function in t and the argument of the δ distribution in (6) has only one zero.

The VD method can be extended to higher-dimensional calculations. In this case, the detector becomes a (hyper)surface the flux through which is given according to (3) by the current density at all points r_d on this surface. The momentum spectra for all points, integrated over the entire (hyper)surface, yield the final momentum spectrum. The choice of the surface depends on the physical problem and the range of momentum components of interest. In the following two sections 3.1 and 3.2, we will test this technique for a moving Gaussian wavepacket in one dimension.

3. Simple test: momentum distribution for a moving Gaussian wavepacket

3.1. Analytical result

The Gaussian wavepacket is prepared at time $t = 0$, centred at $x = 0$ with an initial width Γ and an initial (average) momentum k_0 ,

$$G(x, t = 0) = \left(\frac{1}{\sqrt{\Gamma\pi^{1/4}}} \right) \exp\left(-\frac{x^2}{2\Gamma^2}\right) \exp(ik_0x). \quad (9)$$

The momentum representation of this wavepacket

$$M(k) = \frac{1}{\sqrt{2\pi}} \int_{-\infty}^\infty G(x, t = 0) \exp(-ikx) dx = \frac{\sqrt{\Gamma}}{\pi^{1/4}} \exp\left(-\frac{1}{2}(k_0 - k)^2\Gamma^2\right) \quad (10)$$

leads to the time-dependent, freely propagating wavepacket in coordinate space

$$\begin{aligned} G(x, t) &= \frac{1}{\sqrt{2\pi}} \int_{-\infty}^\infty M(k) \exp\left(i\left(kx - \frac{1}{2}k^2t/\mu\right)\right) dk \\ &= \frac{1}{\pi^{1/4}} \sqrt{\frac{\Gamma}{\Gamma^2 + it/\mu}} \exp\left(-\frac{(x - ik_0\Gamma^2)^2}{2(\Gamma^2 + it/\mu)}\right) \exp\left(-\frac{1}{2}k_0^2\Gamma^2\right). \end{aligned} \quad (11)$$

In order to derive the phase gradient, we rewrite $G(x, t)$ in the form $A(x, t) \exp(i\phi(x, t))$ with the real, time-dependent amplitude

$$A(x, t) = \frac{\sqrt{\Gamma}}{\sqrt{\pi(\Gamma^4 + t^2/\mu^2)}} \exp\left(-\frac{\Gamma^2(x - k_0 t/\mu)^2}{2(\Gamma^4 + t^2/\mu^2)}\right), \quad (12)$$

and a real, time-dependent phase

$$\phi(x, t) = \frac{\Gamma^4 k_0(x - \frac{1}{2}k_0^2 t/\mu) + \frac{1}{2}x^2 t/\mu}{\Gamma^4 + t^2/\mu^2} + \theta(t). \quad (13)$$

The additional global phase $\theta(t)$ is not of interest, since it does not affect the phase gradient. According to (3), (4), we find the ‘local’ momentum at position x_d :

$$k(x_d, t) = \left. \frac{\partial}{\partial x} \right|_{x=x_d} \phi(x, t) = \frac{\Gamma^4 k_0 + x_d t/\mu}{\Gamma^4 + t^2/\mu^2} = \mu v \quad (14)$$

$$\approx \mu x_d/t \quad (x_d t/\mu \gg \Gamma^4 k_0, t^2/\mu^2 \gg \Gamma^4), \quad (15)$$

and the outgoing current

$$j(x_d, t) = \rho(x_d, t)k/\mu = |A(x_d, t)|^2 k/\mu = \frac{\Gamma}{\sqrt{\pi(\Gamma^4 + t^2/\mu^2)}} \exp\left(-\frac{\Gamma^2(x_d - k_0 t/\mu)^2}{\Gamma^4 + t^2/\mu^2}\right) \frac{k}{\mu}. \quad (16)$$

Note, that for the 1D case considered here, there is no need to distinguish between current and current density. Provided that the approximation given above is valid, equation (15) is directly related to a time-of-flight measurement in an experiment with a particle detector placed at position x_d , and the label ‘VD method’ appears appropriate. However, we note that this analogy with the experiment is limited and possibly misleading, since a real ‘measurement’ of the momentum at a fixed position would violate the uncertainty principle. Nevertheless, the phase gradient is related to the momentum distribution. Physically, (13)–(15) show that the leading edge of the Gaussian wavepacket is moving faster than the remaining part, corresponding to normal dispersion.

For sufficiently large t (15) holds and we can use the approximation (8). With $j(x_d, t)$ from (16) and using $t(k) \approx \mu x_d/k$ (15) we finally obtain

$$\frac{dN}{dk} = \frac{\Gamma}{\sqrt{\pi(\Gamma^4 + x_d^2/k^2)}} \exp\left(-\frac{\Gamma^2(x_d - k_0 x_d/k)^2}{\Gamma^4 + x_d^2/k^2}\right) \frac{x_d}{k} \quad (17)$$

$$\approx \frac{\Gamma}{\sqrt{\pi}} \exp(-\Gamma^2(k - k_0)^2) = |M(k)|^2 \quad (x_d^2/k^2 = t^2/\mu^2 \gg \Gamma^4), \quad (18)$$

which is the momentum distribution of the wavepacket (see (10)). The conditions (15), (18) mean that the momentum components of $\Psi(x, t)$ which have the same initial phase at $t = 0$ (9) are dephasing due to the dispersion relation in (11), $E_{\text{kin}} = \frac{1}{2}k^2/\mu$. According to (14), $k(t)$ is equal to k_0 for very small t and exhibits a maximum before it reaches the asymptotic $1/t$ behaviour.

3.2. Numerical result

Let us now consider the numerical test of the VD method for the Gaussian wavepacket. Here, as well as for the other examples in section 4, we use the Crank–Nicholson propagation scheme which provides unconditional numerical stability. The momentum spectra are generated as

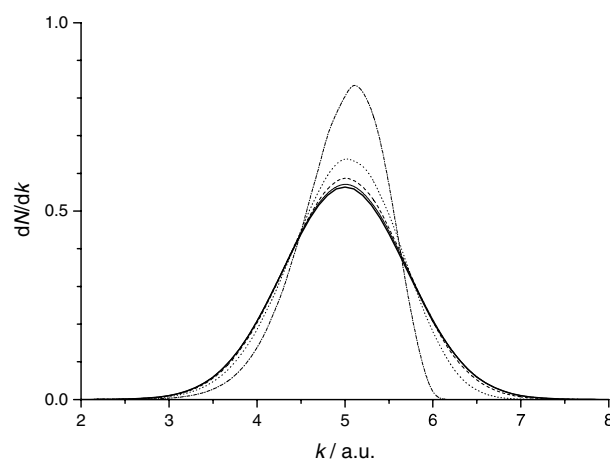


Figure 1. Convergence behaviour of the VD method for a moving Gaussian wavepacket. The exact analytical momentum distribution (10) is given by the thick solid curve. The numerical momentum spectrum is shown for different positions x_d of the VD: — · —, $x_d = 5$; · · · · ·, $x_d = 10$; - - - -, $x_d = 20$; —, $x_d = 50$.

follows. For each time step t_i the phase gradient of the wavepacket at the position x_d of the VD is calculated using a five point formula. According to (5) and (14), the momenta $k_i = k(t_i) = \partial/\partial x[\phi(x, t_i)]_{x_d}$ and $\Delta N/\Delta k(k_i)$ are combined to a histogram. This procedure ensures correct normalization, i.e. the integrated momentum distribution gives the total yield in the corresponding fragmentation channel. Figure 1 shows the convergence behaviour of the VD method with increasing x_d , i.e. the transition from (14) to (15) and (17) to (18), respectively. In the present example we use a Gaussian wavepacket initially centred at $x = 0$ with $\Gamma = 1$, $k_0 = 5$, $\mu = 1$. The propagation was performed up to $t = 25$ with time intervals $\Delta t = 10^{-3}$ on a numerical grid which extends from $x = -20$ to 280 with a grid spacing of $\Delta x = 0.05$. The numerically derived momentum distribution converges quickly towards the analytical result $|M(k)|^2$ as x_d increases from 5 to 50. Once convergence is reached, the numerical distribution no longer depends on x_d (see (18)). The smaller width of the numerical momentum distributions for values of x_d that are smaller than required by approximation (15) is caused by the ‘soliton-like’ behaviour of the wavepacket at small t . In this case we find $k(x_d, t) \approx k_0$ which leads to an (unphysical) δ distribution $\Delta N/\Delta k \approx \delta(k_0)$. Once the dispersion-induced broadening of the wavepacket becomes large compared to the initial width Γ , the numerical momentum distribution also broadens and converges to the analytical result.

4. Numerical applications of the ‘virtual detector’ method

4.1. Momentum distribution of dissociating H_2^+

As a first application, we study dissociation of the H_2^+ molecule following (fast) single ionization of H_2 . The stationary ground state ($v = 0$) nuclear wavefunction of the neutral H_2 molecule is promoted via a vertical (Franck–Condon) transition onto the potential curve of the H_2^+ molecular ion. In our simulation this is achieved by propagating the $v = 0$ state of H_2 on the potential curve of H_2^+ in the electronic ground state. Since the electronic ground state potential curves for H_2 and H_2^+ differ in equilibrium distance and width (Huber and Herzberg 1979),

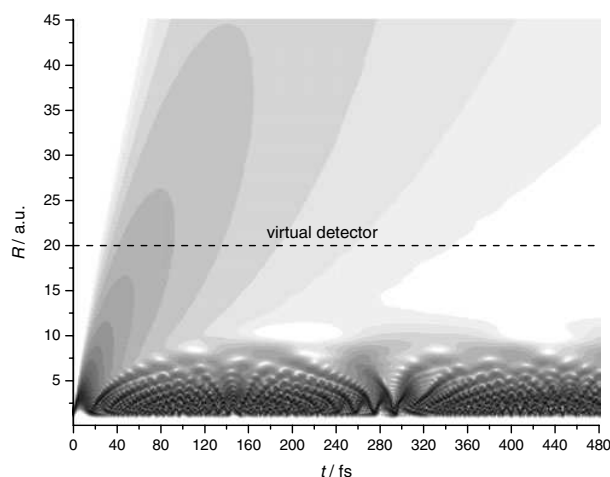


Figure 2. Wavepacket dynamics of H_2^+ following a Franck–Condon transition from the H_2 vibrational ground state. The time evolution of the probability density is shown as a contour plot on a logarithmic grey scale (R : internuclear distance). The position $R_d = 20$ of the VD is indicated by the dashed line. Note the revival of the bound part of the wavepacket at $t = 275$ fs.

the wavefunction becomes a non-stationary wavepacket leading to a *coherent* superposition of many (bound) vibrational states of H_2^+ as well as to dissociation. For comparison, the momentum distribution of the dissociative part of the wavefunction will here be calculated by using (a) standard FT (equation (1)) and (b) the VD method. The 1D numerical grid for the internuclear distance R extends from $R = 0.05$ to 500 with a grid spacing of $\Delta R = 0.05$. The propagation was carried out until $t_{\text{max}} = 2 \times 10^4$ (480 fs) with intervals $\Delta t = 1$.

Figure 2 shows the time evolution of the probability density as a contour plot on a logarithmic grey scale. The FT needs to be taken only for the dissociating part of the wavepacket. Thus, one has to wait until the wavepacket has left the region of bound states, which are localized at $R < 15$. By the time the slowest dissociation components have left that region, the fastest components already reach distances of $R = 420$ which defines a minimum size of the array needed for the FT (figure 3). The sharp cutoff of the wavefront at $R = 420$ is caused by the finite grid spacing which supports free propagation of momentum components up to $k_{\text{max}} \approx 1/\Delta R = 20$ according to Nyquist’s criterion. The corresponding maximum velocity $v_{\text{max}} = k_{\text{max}}/\mu = 20/918 = 2.18 \times 10^{-2}$ gives the position of the wavefront at the end of the propagation at time t_{max} at $R_{\text{max}} = 435$ which is close to the cutoff in figure 3. In contrast to FT, a VD located at $R_d = 20$ requires a much smaller numerical grid extending only to $R = 30$. This includes an absorber located between $R = 20$ and 30, which is adjusted to prevent reflections of the wavepacket at the boundary of the numerical grid. We implemented this absorber as a fourth-order optical potential $V_{\text{opt}} = 0.05(R - 20)^4$ starting at $R = 20$. We also checked the convergence by comparing the numerical momentum spectra for $R_d = 20$ and 40 which show no significant difference. This demonstrates the efficiency of the VD method which reduces the computation time in the present example by more than an order of magnitude. A comparison of the FT result for the fragment momentum spectrum dN/dk with the VD method is given in figure 4. Both results agree very well except for the small superimposed oscillations which are caused by the finite grid size (for the FT) and by the finite number of time steps which causes a statistical error in the VD method. The statistical error can be reduced either by using smaller time steps Δt or by using a set of VDs which extends

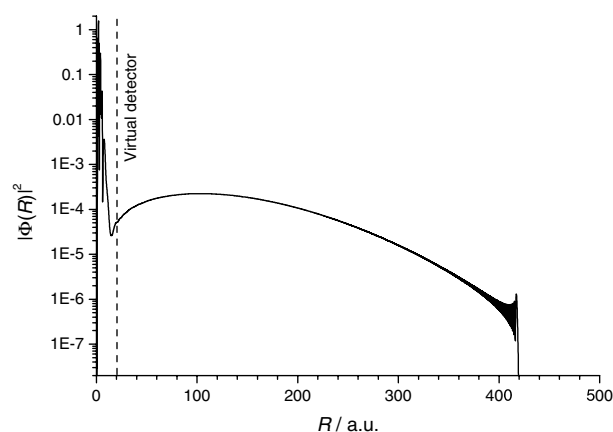


Figure 3. Snapshot (log scale) of the 1D probability density for the H_2^+ nuclei (see also figure 2) as a function of the internuclear distance R at $t = 480$ fs. The bound part of the wavepacket is localized at $R \leq 15$, whereas the dissociative part has already spread from $R = 15$ to 420. The position $R_d = 20$ of the VD is indicated by the dashed line. Note the sharp cutoff of the wavefront at $R = 420$ due to the finite grid spacing ($\Delta R = 0.05$).

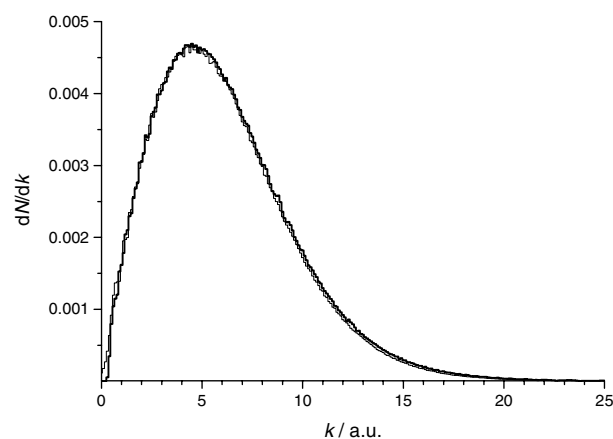


Figure 4. Momentum spectrum for dissociation of H_2^+ following a Franck–Condon transition from the H_2 vibrational ground state. Thick solid curve: VD method; thin solid curve: FT result.

over a finite array of grid points. The latter method was found to be much more effective with respect to computation time, since it only requires the calculation of the phase gradient at a set of fixed positions x_d . The time propagation is a matrix operation on the entire numerical grid and, thus, reduction of Δt is much more time consuming.

4.2. Quiver motion of an electron ionized by a strong laser field

In the second numerical example, we examine the strong-field ionization of a 1D model hydrogen atom, in particular, the effect of the quiver motion of the electron on the momentum distribution. The mean quiver energy of an electron in the presence of the laser of electric field strength \mathcal{E} and frequency ω is expressed in terms of the ‘ponderomotive energy’ $U_p = \mathcal{E}^2/4\omega^2$.

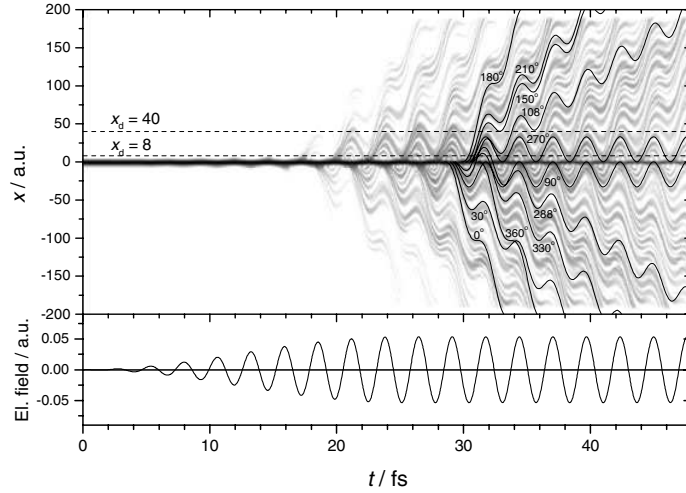


Figure 5. Strong-field ionization of a 1D model hydrogen atom by a 0.1 PW cm^{-2} intensity, 800 nm CW laser (with 25 fs ramp): contour plot (logarithmic grey scale) of the time evolution of the electron probability density. The positions of the VD are indicated by the broken lines. Selected classical trajectories starting within one optical cycle are shown as solid curves. The labels give the corresponding phases relative to the $\sin(\omega t)$ CW laser electric field.

The electron–nucleus interaction of the atom is modelled by a soft-core Coulomb potential (Su and Eberly 1991) $-1/\sqrt{x^2 + a^2}$ where the parameter $a = 1.4$ is adjusted to the ionization potential of hydrogen. The 1D grid extends from $x = -200$ to 200 with a grid spacing of $\Delta x = 0.2$. Fourth-order optical potential absorbers were used covering the first and last 100 grid points.

The quiver motion may lead (depending on the phase of the laser field, when the electron was ionized) to a rescattering of the electron (Corkum 1993, Paulus *et al* 1994, Kulander *et al* 1995, Feuerstein *et al* 2000). Figure 5 shows the time-dependent electron probability density for the 1D model hydrogen atom interacting with a CW 800 nm laser at 0.1 PW cm^{-2} with a 25 fs \sin^2 ramp. For the propagation, 1100 time steps were used per optical cycle. Interestingly, the outgoing electron ‘jets’ exhibit a structure similar to classical electron trajectories in a laser field (see, e.g., figure 1 in Feuerstein *et al* 2000). For comparison, we show selected classical trajectories starting within one optical cycle for different phases of the oscillating laser field ($\sin(\omega t)$). Rescattering occurs for phases $90^\circ \leq \omega t < 180^\circ$ and $270^\circ \leq \omega t < 360^\circ$, respectively. The VD method allows us to extract the (not directly observable) momenta of the quiver motion. In order to demonstrate the effect of the quiver motion, we consider the momentum distributions derived for two different positions of the VD. In the first case, the VD is placed at a distance $x_d = 8$ from the atomic nucleus. This distance is smaller than the classical quiver amplitude $x_q = \mathcal{E}/\omega^2 = 5.3 \times 10^{-2}/0.057^2 = 16.4$, but lies outside the region with significant density of bound states which would otherwise disturb the spectrum. At this position close to the nucleus, rescattering events influence the momentum distribution (solid curve in figure 6). Negative momenta (note that $x_d > 0$) are observed with a cutoff close to the classical maximal recollision momentum (Corkum 1993) $k_{\text{rec}} = -\sqrt{2} \times 3.17U_p = -1.2$.

If the VD is placed at $x_d = 40$ we exclude negative drift momenta, since only the corresponding classical trajectories starting at $90^\circ < \omega t < 270^\circ$ reach the VD. Thus, the momentum distribution is shifted towards positive momenta (the dashed curve in figure 6)

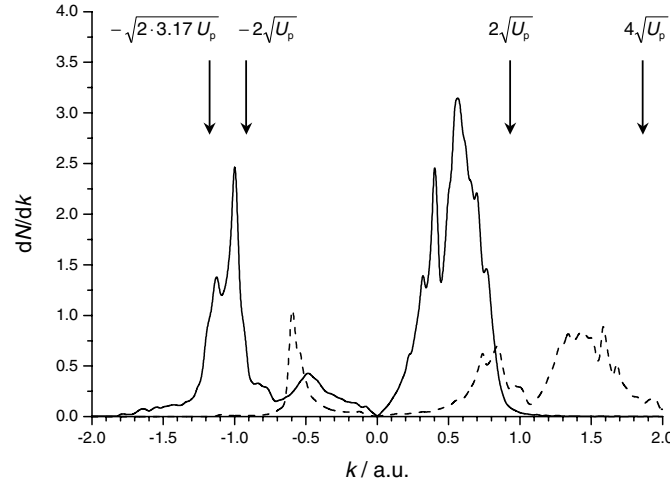


Figure 6. Momentum distributions for an electron after strong-field ionization of a 1D model hydrogen atom. Laser parameters: 0.1 PW cm^{-2} intensity, 800 nm wavelength, CW with a 25 fs ramp. The VD is placed at $x_d = 8$ (solid curve) and $x_d = 40$ (dashed curve), respectively. Typical momenta for an electron in a laser field are indicated by arrows (also see the text).

and extends up to the upper limit for the classical motion of an electron in a strong laser field $k_{\text{max}} = 4\sqrt{U_p} = 1.9$. Here, the drift and quiver momenta (the maximum value of both being $2\sqrt{U_p} = 0.95$) add up constructively. We note that the asymmetry of both spectra shown in figure 6 with respect to $k = 0$ is not caused by an absolute phase effect, but rather by the fact that we considered only one direction, i.e. we used only one VD. Absolute phase effects are negligible in this example since the laser field is turned on sufficiently slowly and, at 0.1 PW cm^{-2} , the ionization rate is relatively small, i.e. the ionization occurs over many optical cycles without depletion of the bound states. A VD placed at $-x_d$ would yield a mirror image of the corresponding momentum distribution. Thus, the sum of the spectra for VDs placed at x_d and $-x_d$ will give a symmetric spectrum since absolute phase effects are negligible.

5. Conclusion

In this paper we proposed a new method to extract momentum and kinetic energy distributions from time-dependent wavepacket propagation calculations. Compared to the established FT method which uses the spatial dependence of the wavepacket at a fixed time, this new VD method examines the time-dependent behaviour of the wavepacket at a fixed position x_d . Thus, the size of the spatial array needed to extract the momentum spectrum can be reduced significantly. As a test, for 1D Gaussian wavepackets, the equivalence with FT was shown analytically. In numerical examples we demonstrate that compared to FT, the computation time can be reduced by more than a factor of ten. In addition to being faster than the FT method, the use of the VD method provides momentum information that is not otherwise available, as shown in our example for the quiver motion of an electron ionized by a strong laser field.

Acknowledgments

This work was supported in part by the National Science Foundation (grant no PHY-0071035) and the Division of Chemical Sciences, Office of Basic Energy Sciences, Office of Energy

Research, US Department of Energy. BF acknowledges the financial support in the form of a Research Scholarship provided by the Deutsche Forschungsgemeinschaft.

References

- Bandrauk A D and Chelkowski S 2001 *Phys. Rev. Lett.* **87** 273004
- Borisov A G, Kazansky A K and Gauyacq J P 1999 *Phys. Rev. B* **59** 10935
- Chelkowski S, Conjusteau A, Zuo T and Bandrauk A D 1996 *Phys. Rev. A* **54** 3235
- Corkum P B 1993 *Phys. Rev. Lett.* **71** 1994
- Dundas D, Taylor K T, Parker J S and Smyth E S 1999 *J. Phys. B: At. Mol. Opt. Phys.* **32** L231
- Feuerstein B, Moshhammer R and Ullrich J 2000 *J. Phys. B: At. Mol. Opt. Phys.* **33** L823
- Hermann M R and Fleck Jr J A 1988 *Phys. Rev. A* **38** 6000
- Huber K P and Herzberg G 1979 *Molecular Structure and Molecular Spectra IV. Constants of Diatomic Molecules* (New York: Van Nostrand-Reinhold)
- Keller A 1995 *Phys. Rev. A* **52** 1450
- Kosloff R 1994 *Annu. Rev. Phys. Chem.* **45** 145
- Kulander K C, Cooper J and Schafer K J 1995 *Phys. Rev. A* **51** 561
- Kulander K C, Mies F H and Schafer K J 1996 *Phys. Rev. A* **53** 2562
- Lein M, Gross E K U and Engel V 2000 *J. Phys. B: At. Mol. Opt. Phys.* **33** 433
- Liu W C, Eberly J H, Haan S L and Grobe R 2000 *Phys. Rev. Lett.* **83** 520
- Neuhauser D 1992 *Chem. Phys. Lett.* **200** 173
- Parker J S, Moore L R, Merhag K J, Dundas D and Taylor K T 2001 *J. Phys. B: At. Mol. Opt. Phys.* **34** L69
- Paulus G G, Becker W, Nicklich W and Walther H 1994 *J. Phys. B: At. Mol. Opt. Phys.* **27** L703
- Su Q and Eberly J H 1991 *Phys. Rev. A* **44** 5997
- Thumm U 2002 *22nd Int. Conf. on the Physics of Photonic, Electronic and Atomic Collisions (Santa Fe, NM)* ed S Datz *et al* (Princeton, NJ: Rinton Press) p 592 Book of invited papers
- Walsh T D G, Ilkov F A, Chin S L, Châteauneuf F, Nguyen-Dang T T, Chelkowski S, Bandrauk A D and Atabek O 1998 *Phys. Rev. A* **58** 3922